Contrasting nonphotochemical quenching patterns under high light and darkness aligns with light niche occupancy in Arctic diatoms

Dany Croteau, Sébastien Guerin, Flavienne Bruyant, Joannie Ferland, Douglas A Campbell, Marcel Babin, Johann Lavaud

LIMNOLOGY and OCEANOGRAPHY

ASLO

Limnol. Oceanogr. 9999, 2020, 1–15

doi: 10.1002/lno.11587

Contrasting nonphotochemical quenching patterns under high light and darkness aligns with light niche occupancy in Arctic diatoms

Dany Croteau,[1]* **Sébastien Guérin**,[1] **Flavienne Bruyant**,[1] **Joannie Ferland**,[1] **Douglas A. Campbell**,[2] **Marcel Babin**,[1] **Johann Lavaud**[1]

[1]Takuvik UMI 3376 CNRS/ULaval and Québec-Océan, Département de Biologie, Pavillon Alexandre Vachon, Université Laval, Québec, Québec, Canada

[2]Biology Department, Mount Allison University, Sackville, New Brunswick, Canada

Abstract

Over the seasons, Arctic diatom species occupy shifting habitats defined by contrasting light climates, constrained by snow and ice cover dynamics interacting with extreme photoperiod and solar angle variations. How Arctic diatom photoadaptation strategies differ across their heterogeneous light niches remains a poorly documented but crucial missing link to anticipate Arctic Ocean responses to shrinking sea-ice and increasing light. To address this question, we selected five Arctic diatom species with diverse life traits, representative of distinct light niches across the seasonal light environment continuum: from snow-covered dimly lit bottom ice to summer stratified waters. We studied their photoacclimation plasticity to two growth light levels and the subsequent responses of their nonphotochemical quenching (NPQ) and xanthophyll cycle to both dark incubations and light shifts. We deciphered NPQ and xanthophyll cycle tuning in darkness and their light-dependent induction kinetics, which aligned with species' light niche occupancy. In ice-related species, NPQ was sustained in darkness and its induction was more reactive to moderate light shifts. Open-water species triggered strong NPQ induction in darkness and reached higher maximal NPQ under high light. Marginal ice zone species showed strong adaptation to light fluctuations with a dark response fine-tuned depending upon light history. We argue these traits are anchored in diverging photoadaption strategies fostering Arctic diatom success in their respective light niches.

Profound phenological change defines high latitude ecosystems. The Arctic Ocean is the epitome of seasonal habitat transformation as winter darkness and snow-covered sea-ice gradually yield to summer with intensely illuminated open waters under long photoperiods (Fig. 1). Despite drastic environmental cycles and freezing temperatures, life thrives in the Arctic Ocean, thanks in part to diatom microalgae, the main primary producers (Poulin et al. 2011). Arctic diatom annual productivity climaxes during the spring-to-summer transition through successive blooms underneath the ice cover and then in the marginal ice zone. These blooms are roughly equally productive (Mayot et al. 2018) but are dominated by different taxonomic assemblages (Lafond et al. 2019). The ongoing warming of the Arctic increases light available for photosynthesis by promoting thinner and shrunken snow and sea-ice cover. While increasing irradiance (combined to increasing nitrogen flux) currently boosts the annual productivity of the Arctic Ocean (Lewis et al. 2020), it could also shift its seasonal peak further toward under-ice conditions, with great ecological consequences (Post et al. 2013). Because of their pronounced shade adaptation, a brighter future Arctic Ocean could be detrimental to lipid-rich sympagic (sea-ice) diatoms, a central link in the bentho-pelagic food chain (Leu et al. 2010). Since the fate of the Arctic Ocean largely depends upon sympagic and planktonic diatom spring bloom responses to climate perturbations, efforts are being deployed to understand determinants of their blooming (Massicotte et al. 2020).

Over their seasonal succession, Arctic diatoms collectively exploit a strong light environment continuum coupled to habitat shifts (Fig. 1 and Supporting Information Fig. S1). In Baffin Bay, the productive season begins early in spring within the bottom centimeters of the snow-covered sea-ice (Habitat 1, Fig. 1), under extremely weak irradiances (Hancke et al. 2018). Pennate diatoms dominate this sympagic biomass, frequently with major contributions from *Nitzschia frigida* (Poulin et al. 2011)

*Correspondence: dany.croteau.3@ulaval.ca

Additional Supporting Information may be found in the online version of this article.

Special Issue: Biogeochemistry and Ecology across Arctic Aquatic Ecosystems in the Face of Change
Edited by: Peter J. Hernes, Suzanne Tank and Ronnie N. Glud

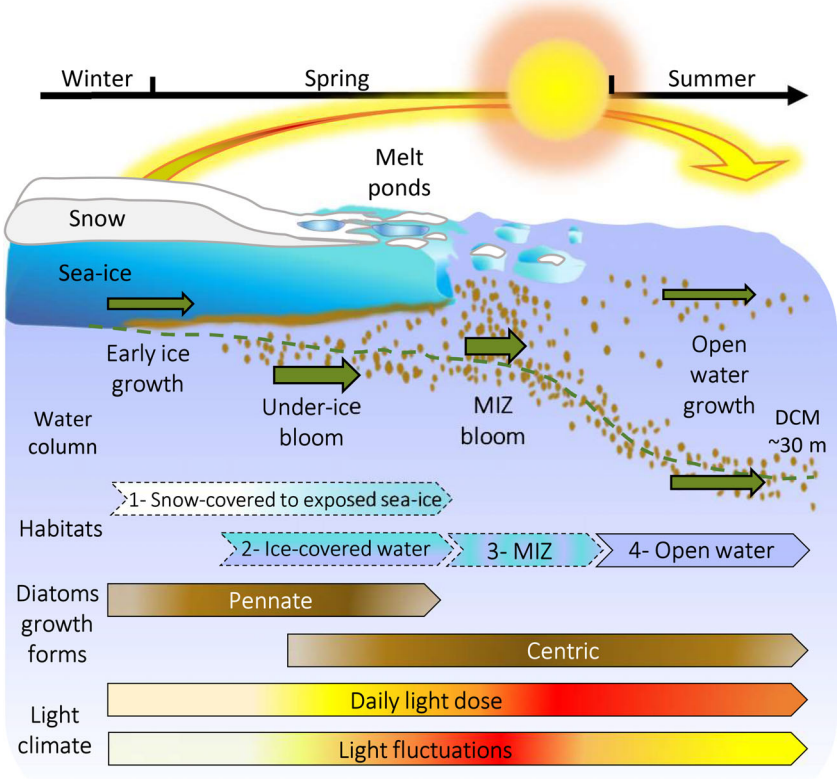

Fig. 1. Schematic representation of a typical Arctic diatom seasonal succession in Baffin Bay (67.48 N; 63.79 W) through four shifting habitats along an annual light environment continuum. Daily light dose corresponds to atmospheric radiation measured above ocean level and is governed by photoperiod and solar angle-of-incidence (*see* Supporting Information Fig. S1). Light fluctuations frequency and amplitude increase with snowmelt and sea-ice cover heterogeneity. Pennate diatoms dominate the sea-ice biomass and centric diatoms dominate the phytoplankton (*see* Introduction). See (Massicotte et al. 2020) for in depth description of the physicochemical parameters determining phytoplankton under-ice and marginal ice zone (MIZ) spring blooms onset in Baffin Bay. Dashed green line represents the deep chlorophyll maximum (DCM).

(Table 1). As snow melts, light transmission to the ice-covered ocean surface (Habitat 2) increases heterogeneously due to emerging icescape features (melt ponds, leads, etc.) (Katlein et al. 2019). Upon this exposure to more intense and fluctuating irradiances, under-ice drifters, like the dual sympagic/planktonic *Fragilariopsis cylindrus*, start blooming (Arrigo et al. 2012). When nitrate supply remains sufficient to sustain it, productivity culminates at the marginal ice zone (Habitat 3), in the surface layer stratified by meltwater and exposed to unsteady light interacting with fragmenting ice floes (Mayot et al. 2018). This locally brief bloom event progresses latitudinally, dominated by "bloom and bust" centric species like *Thalassiosira gravida* (Poulin et al. 2011). As photoperiod lengthens and the solar angle-of-incidence increases, planktonic growth in open water (Habitat 4) continues under increasing daily irradiance. Compromising between nutrient availability and surging grazing pressure, diatoms exploit different depths. For example, long enduring species like *Chaetoceros neogracilis* and *Chaetoceros gelidus* dominate the subsurface ($\sim$ 3 m) and deep ($\sim$ 30 m) chlorophyll (Chl) maxima, respectively (Balzano et al. 2017). The habitat zone and depth where a species can be found in relative abundance is referred to as its light niche from here onward (Table 1).

To maintain productivity and growth in these contrasting niches, Arctic diatoms must constantly balance light energy harvesting and photochemically driven carbon fixation. When photochemical electron transport outstrips downstream assimilatory reactions, net photodamage can ensue (Campbell and Serôdio 2020). With subzero temperatures slowing down photosynthetic enzymes and repair processes, the margin between net photoproduction and photoinhibition shrinks (Verhoeven et al. 2018). The molecular toolkit evolved by photoautotrophs to optimize growth in a specific light niche represents their photoadaptation strategy. It comprises: (1) Day to season scale photoacclimative processes operating over generational time scales, including large modulations of light harvesting pigments and assimilatory enzymes like Rubisco in polar diatoms (Lacour et al. 2017); and (2) Faster responding (seconds to hours) photoprotective mechanisms dissipating excessive light energy and mitigating photodamage. In diatoms, the multicomponent nonphotochemical quenching (NPQ) serves as the main short-term photoprotection (Buck et al. 2019). In diatoms, the central NPQ component is *qE* ("energy-dependent" quenching) whose dynamic regulation relies upon synergistic interactions between a transthylakoidal proton gradient,

Table 1. Arctic diatom species investigated in this study with their light niches, defining life traits and strain reference (habitats refer to Fig. 1).

Light niches				Life traits				
Habitats	Depth adaptation (m)	Species	Life forms	Growth forms	Bloom formation	Colonial	Biovolume (μm^3)	Strain references
1	Ice-water interface	*Nitzschia frigida* *N.f.*	Sympagic	P	Yes	Yes	325	A. Juhl
1–2–3	Unknown	*Fragilariopsis cylindrus* *F.c.*	Dual form	P	Yes	Yes	35	CCMP1102
2–3	30	*Thalassiosira gravida* *T.g.*		C	Yes	Yes	15,000	RCC5318
3–4	3	*Chaetoceros neogracilis* *C.n.*	Planktonic	C	No	No	45	RCC2278
3–4	30	*Chaetoceros gelidus* *C.g.*		C	Yes	Yes	95	RCC2046

C, centric growth form; CCMP, culture collection of marine phytoplankton; P, pennate growth form; RCC, Roscoff culture collection.

the enzymatic conversion of the xanthophyll pigment diadinoxanthin to diatoxanthin through the "xanthophyll cycle," and differential expression of specific LHCx proteins of the light-harvesting complex family (Buck et al. 2019). In diatoms, and other marine phototrophs, xanthophyll cycle and NPQ amplitudes reflect both light niche adaptation (Petrou et al. 2011; Barnett et al. 2015) and light history acclimation, which modulates xanthophyll pigment pool size (Galindo et al. 2017). Moreover, defining microalgal functional groups by their NPQ and xanthophyll cycle patterns has proven a powerful tool to enhance modeling of seasonal species succession (Polimene et al. 2014) and global carbon fixation (Álvarez et al. 2019).

Compared to their temperate counterparts, important distinctions among polar diatom photoadaptation strategies are emerging (Lacour et al. 2017, 2020). In addition to dynamic NPQ-*qE*, sustained NPQ (NPQ_S) together with high diatoxanthin amounts are commonly reported both in polar diatom cultures (Lacour et al. 2018) and in sea-ice communities (Galindo et al. 2017). A conceptual parallel has been drawn with overwintering evergreen trees which induce long-lasting quenching (termed *qZ*) (Verhoeven et al. 2018) to cope with a similar stress combination of changing light conditions and persistent low temperature (Lacour et al. 2018). In *F. cylindrus* and *T. gravida*, sustained NPQ may provide extra photoprotection when low light-adapted cells are suddenly trapped beneath uncovered sea-ice and/or in a stratified surface layer (Kropuenske et al. 2009). Potentially complementary to NPQ-*qE* and sustained NPQ, a nonphotochemically driven diatoxanthin accumulation and concomitant NPQ increase after 1 month of dark incubation has been reported in *C. neogracilis* (Lacour et al. 2019). This dark induction of NPQ could support rapid photophysiological recovery upon light exposure following polar winter or transport to surface waters. We hypothesized that these contrasting and unusual NPQ regulations in different polar diatoms may indicate an underappreciated role of recurrent darkness events caused by the shifting interactions of extreme photoperiod, punctuated snowfalls, advective transport underneath sea-ice, and deep vertical mixing toward shaping Arctic diatom photoadaptation strategies.

Notwithstanding these remarkable photophysiological features of polar diatoms, no study has tested, across a range of species, whether the contrasting seasonal light niches of Arctic diatoms are strong predictors of their photoadaption strategies. To address this gap in knowledge, we selected five Arctic diatom species derived from contrasting seasonal light niches, which exhibit diverse life traits potentially influencing photophysiology (Table 1). Kvernvik et al. (2020) recently showed that sympagic *N. frigida* is less tolerant to prolonged light stress than planktonic *Thalassiosira hyalina* even though both species heavily rely on NPQ and xanthophyll cycle. With an expanded selection of species from contrasting seasonal light niches, we set out to: (1) Compare the rapidly responding induction kinetics of NPQ upon light shifts and their coupling to the xanthophyll cycle; and (2) Document the occurrence and interplay among perplexing dark NPQ patterns in Arctic diatoms (Lacour et al. 2018, 2019). Longer-term photoprotective mechanisms, including the photosystem II repair cycle, will be addressed in a forthcoming paper using the same panel of species. We propose a strong evolutionary driving role of the sea-ice cover in promoting contrasted NPQ and xanthophyll cycle patterns, embedded in a survivalist photoadaptation strategy in sympagic diatom species as opposed to a more dynamic competition-oriented strategy of open-water planktonic diatoms.

Materials and methods

Diatoms culturing

Five Arctic diatom strains derived from contrasting seasonal light niches were selected (Table 1). Cells were grown in

seawater (Baffin Bay 67.48 N; 63.79 W) which was first sterilized by filtration (0.2 μm) and enriched with f/2 medium. Culture triplicates of 600 mL were diluted with fresh medium every 2 d to achieve balanced growth. Cultures were illuminated by LEDs continuously to avoid NPQ variability related to polar diatom diurnal physiological rhythmicity (S. Guérin and J. Lavaud pers. comm.). We chose LEDs for their emission spectrum closer to natural light fields underneath sea-ice than conventional culture chamber light bulbs (Supporting Information Fig. S2). Cells were acclimated under two growth light levels (*gE*): 15 (gE_{15}) and 50 (gE_{50}) μmol photons m^{-2} s^{-1}, as measured with a US-SQS/L spherical quantum sensor (Walz, Germany). We chose 15 μmol photons m^{-2} s^{-1} to deliver a typical daily light dose (1.23 mol photons m^{-2} d^{-1}) for sea-ice bottom algae in June as snowmelt initiates in Baffin Bay (Supporting Information Fig. S1). We chose 50 μmol photons m^{-2} s^{-1} to deliver a daily light dose (4.32 photons m^{-2} d^{-1}) typical for open water or at the ice-water interface when the melt pond proportion increases (Supporting Information Fig. S1). While 50 μmol photons m^{-2} s^{-1} could be slightly limiting for late seasonal *Chaetoceros* species, it was chosen to limit photoinhibitory quenching across the five strains and provide a comparison point of photoacclimation plasticity together with 15 μmol photons m^{-2} s^{-1}. Culture maintenance and experiments were all conducted in a 0°C lab.

Cell growth and acclimation monitoring

Cell numbers and diameters were measured using a Beckman Multisizer 4 Coulter Counter (Miami, Florida, U.S.A.) except for *N. frigida* which required microscopy counting (Utermöhl method). Cellular chlorophyll *a* (Chl *a*) (extracted in acetone 90 : 10, vol : vol, and estimated with a 10 AU fluorometer; Turner Designs, San Jose, California, U.S.A.), cell diameter and growth rate were monitored every 2 d. Spherical biovolumes were calculated for all species but *N. frigida*, for which the "cylinder + 2 half spheres" formula was used.

Pigment concentrations

Culture samples of 15 mL were filtered onto GF/F filters (Whatman®, 0.7 μm, 25 mm), flash frozen in liquid nitrogen and stored at −80°C until analysis. Samples extracted in 100% methanol were mixed (70 : 30, vol : vol) with a buffer solution (tetrabutylammonium acetate [28 mmol L^{-1}]) following a method adapted from Ras et al. (2008). Pigment contents were measured using high-performance liquid chromatography with a Zorbax Eclipse XDB-C8 3.5 μm column (Agilent Technologies, Santa Clara, California, U.S.A.).

NPQ and xanthophyll cycle behavior over 48 h dark incubation experiment

Because NPQ of Chl *a* fluorescence can be long-lasting in polar diatoms (Lacour et al. 2018) and an initial underestimation of maximum fluorescence (F_M) (all parameters explained in Supporting Information Table S3) hinders subsequent calculation of fluorescence-derived photophysiological parameters, we first monitored the relaxation kinetics of NPQ and related xanthophyll cycle in darkness. Although low light incubation is more efficient in relaxing NPQ in diatoms, we used darkness (see also Lacour et al. 2018) to: (1) Avoid perturbing photochemistry before subsequent light treatments in these extremely shade-adapted Arctic diatoms (Lacour et al. 2017) (see below); and (2) Simultaneously investigate their responses to the transient dark events which they frequently face in the Arctic environment (*see* Introduction). Triplicates of cultures were therefore incubated in darkness for 48 h. Samples of 3 mL were taken repeatedly (*see* "Results" section) and immediately transferred to a Pulse-Amplitude-Modulation fluorometer (Water-PAM, Walz). Because dark-adapted minimum and maximum fluorescence yield (F_0 and F_M, respectively) were generally not reached after a customary 20 min dark relaxation, we adjusted the nomenclature and the calculation of different fluorescence indices as follows. Minimum and maximum fluorescence dependent upon dark incubation time were termed F_t and F_{Mt}, respectively, where t is time in darkness, and then used to calculate the progression of photosystem II quantum yield over increasing time of dark incubation:

$$F_{Vt}/F_{Mt} = (F_{Mt} - F_t)/F_{Mt}$$

The highest F_{Mt} value measured during the 48 h dark incubation was considered as "true" F_M and used to calculate ϕNPQ post facto:

$$\phi\text{NPQ} = F_t/F_{Mt} - F_t/F_M$$

The 0–1 bounded ϕNPQ parameter was chosen over the Stern-Volmer NPQ which departs from a linear relation to excitation dissipation, particularly for high values (Buck et al. 2019). Furthermore, ϕNPQ responds to variations in F_t unlike the Stern-Volmer NPQ. The values of F_t and F_{Mt} are shown in Supporting Information Fig. S4. In parallel, 15 mL samples were repeatedly collected from the dark incubated diatom cultures for pigment analysis. To further investigate the special case of *T. gravida* (*see* "Results" section), prolonged relaxation under 1 μmol photons m^{-2} s^{-1} was also monitored similarly in *T. gravida* only.

NPQ and xanthophyll cycle induction kinetics upon light shift

Fresh culture triplicate samples were then taken from the growth cultures and dark acclimated for the specific time determined for their respective species and growth light to maximally relax NPQ, as defined during previous 48 h dark incubations. These relaxation times ranged between 20 min (*C. gelidus*) and 24 h (*F. cylindrus*) of darkness (Supporting Information Fig. S4). Independent 17.5 mL culture subsamples were transferred to a light chamber (DW3, Hansatech Instruments, UK) linked to a Xenon-PAM (Walz) by an optic fiber to perform a nonsequential light curve. A first saturating pulse

(3000 μmol photons m^{-2} s^{-1}, 0.8 s) was fired to assess F_0, F_M, and F_V/F_M on an optimally dark-acclimated subsample. Each independent subsample was then exposed during 5 min to one specific light intensity (nine steps from 6 to 1850 μmol photons m^{-2} s^{-1}). After 5 min of illumination, steady-state fluorescence (F') was recorded and then a saturating pulse was fired to measure maximal light-exposed fluorescence (F_M'). Fluorescence measurements from all subsamples were used to fit relative electron transport vs. light intensity (yielding the "photoacclimation parameter," E_k) and ϕNPQ vs. light intensity curves (Serôdio and Lavaud 2011). Three parameters derived from a ϕNPQ fitted curve describe its shape and can be linked to a species' photoadaptation strategy (Barnett et al. 2015); ϕNPQ fitted maximal value (ϕNPQ_M), which thereafter is designed as "maximal ϕNPQ," light intensity (E) for half-saturation ($E50\phi NPQ$) and the sigmoidicity coefficient ($n\phi NPQ$) distinguishing between logarithmical ($n \sim 1$) and sigmoidal ($n \sim 2$) induction of ϕNPQ with increasing light (Supporting Information Table S3). After light exposure, each subsample was quickly filtered and flash frozen in liquid nitrogen for further pigment analysis. The same curve fitting approach was used to parameterize changes in newly generated diatoxanthin (ΔDT) and changes in xanthophyll pigment de-epoxidation state (ΔDES = ΔDT/[DD + DT] × 100) vs. light intensity, where DD is diadinoxanthin (Supporting Information Table S3). This experiment was chosen to determine how, depending upon growth light level acclimation, Arctic diatoms trigger short-term photoprotection to cope with fast light fluctuations, generated by interactions of snow and sea-ice with incident light in their habitats.

Statistical tests

We first used unpaired *t*-tests to reveal significant differences in means of pigment content (Supporting Information Table S5) and photophysiological parameters (Table 2 and Supporting Information Table S6) within a same species between the two growth light levels to test photoacclimatory plasticity. A two-way ANOVA followed by Tukey's HSD post-hoc test was used with growth light and species as independent factors to determine the effects of these factors and their interaction upon photophysiological parameters. We regrouped the species showing no significant differences for each parameter to see how they align with light niche occupancy (Supporting Information Table S7).

Results

Growth and pigment content

Growth rates were at least 25% higher under growth light of 50 (gE_{50}) compared to 15 μmol photons m^{-2} s^{-1} (gE_{15}) in both open water *Chaetoceros* species (Table 2). In the other species, growth rates under 50 μmol photons m^{-2} s^{-1} were either similar (*F. cylindrus* and *T. gravida*) or lower (*N. frigida*) compared to 15 μmol photons m^{-2} s^{-1}. As expected, all species had a lower

Table 2. Growth, photosynthetic, NPQ, and xanthophyll cycle (XC) parameters derived by fitting nonsequential light curves as described in Serôdio and Lavaud (2011) (all chlorophyll fluorescence parameters are defined in Supporting Information Table S3). Asterisks indicate significant difference within the same species between gE ($P < 0.05$, unpaired *t*-test). Data are mean values $N = 3$, ± SE. Additional photophysiological parameters can be found in Supporting Information Table S6 and interspecies statistic tests results in Supporting Information Table S7.

		Growth parameters		Photosynthetic parameters		NPQ parameters			XC parameters	
Sp.	gE	μ	F_V/F_{MS}	F_V/F_{Mmax}	E_k/gE	ϕNPQ_M	$E50\phi NPQ/gE$	$E50\phi NPQ/E_k$	ΔDT_M	$E50\phi NPQ/E50\Delta DT$
N.f.	15	$0.17 \pm 7 \times 10^{-3}$	0.66 ± 0.01	0.67 ± 0.01	2.00 ± 0.10	0.46 ± 0.03	4.44 ± 0.41	2.22 ± 0.19	1.27 ± 0.27	1.40 ± 0.37
	50	$0.12 \pm 3 \times 10^{-3}$*	$0.62 \pm 3 \times 10^{-3}$*	$0.64 \pm 1 \times 10^{-3}$*	0.82 ± 0.07*	0.73 ± 0.01*	1.71 ± 0.22*	2.07 ± 0.18	3.73 ± 0.16*	0.64 ± 0.02
F.c.	15	$0.19 \pm 6 \times 10^{-3}$	0.57 ± 0.01	0.62 ± 0.01	1.42 ± 0.13	0.56 ± 0.01	3.15 ± 0.26	2.24 ± 0.20	3.60 ± 0.13	0.56 ± 0.08
	50	$0.20 \pm 3 \times 10^{-3}$	0.56 ± 0.01	$0.61 \pm 2 \times 10^{-3}$	0.84 ± 0.05*	0.71 ± 0.02*	1.95 ± 0.16*	2.36 ± 0.30	13.7 ± 1.48*	0.34 ± 0.03
T.g.	15	$0.16 \pm 1 \times 10^{-2}$	$0.56 \pm 5 \times 10^{-3}$	0.60 ± 0.01	2.26 ± 0.13	0.46 ± 0.01	5.32 ± 0.72	2.56 ± 0.15	0.55 ± 0.06	2.10 ± 0.31
	50	$0.18 \pm 1.7 \times^{-3}$	0.51 ± 0.02*	0.58 ± 0.01	0.65 ± 0.06*	0.56 ± 0.03*	1.03 ± 0.07*	1.59 ± 0.03*	1.25 ± 0.09*	1.89 ± 0.42
C.n.	15	0.23 ± 0.01	$0.63 \pm 2 \times 10^{-3}$	0.69 ± 0.02	5.85 ± 0.15	0.68 ± 0.03	11.48 ± 1.18	1.96 ± 0.17	2.14 ± 0.20	1.28 ± 0.04
	50	0.30 ± 0.01*	0.64 ± 0.01*	$0.68 \pm 5 \times 10^{-3}$	2.81 ± 0.03*	0.79 ± 0.01*	7.17 ± 0.54*	2.55 ± 0.19	9.41 ± 0.33*	0.63 ± 0.04*
C.g.	15	0.20 ± 0.04	$0.66 \pm 4 \times 10^{-3}$	$0.67 \pm 4 \times 10^{-3}$	4.53 ± 0.29	0.70 ± 0.02	10.51 ± 0.66	2.33 ± 0.18	0.86 ± 0.11	1.40 ± 0.14
	50	$0.32 \pm 7 \times 10^{-3}$*	0.61 ± 0.01*	0.62 ± 0.01*	1.72 ± 0.03*	0.81 ± 0.01*	4.10 ± 0.30*	2.39 ± 0.17	2.93 ± 0.43*	1.01 ± 0.08

N.f., Nitzschia frigida; F.c., Fragilariopsis cylindrus; T.g., Thalassiosira gravida; C.n., Chaetoceros neogracilis; C.g., Chaetoceros gelidus; μ, growth rate (expressed in d^{-1}); F_V/F_{MS}, 5 min dark adapted quantum yield of photosystem II (PSII); F_V/F_{Mmax}, maximal dark adapted quantum yield of photosystem II; E_k, photoacclimation parameter; ϕNPQ_M, maximum fitted NPQ quantum yield; *E50, E* for half-saturation of maximal parameter value; ΔDT_M, new diatoxanthin generation fitted maximum (expressed in mol, 100 mol Chl a^{-1}).

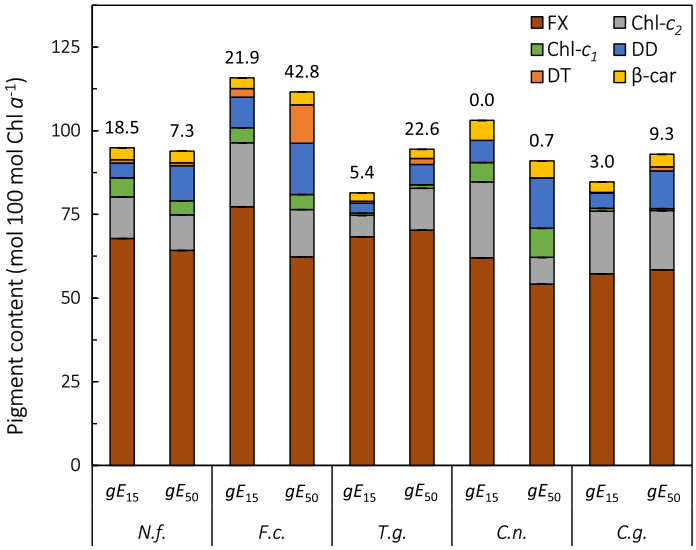

Fig. 2. Species pigment content (in molar ratio to Chl *a*) and de-epoxidation state (in percentage written above histogram bars) acclimated to growth light (*gE*) of 15 or 50 μmol photons m^{-2} s^{-1} but measured after 5 min of dark incubation. Pigments are fucoxanthin (FX), Chl c_1, Chl c_2, diadinoxanthin (DD), diatoxanthin (DT), and β-carotene (β-car). Diatom species abbreviations are in Table 1. Data are mean values N = 3, ± SE. See Supporting Information Table S5 for pigment content values and statistical differences within the same species between *gE*, and Supporting Information Table S7 for interspecies statistic tests results.

cellular Chl *a* concentration under 50 compared to 15 μmol photons m^{-2} s^{-1}, but the difference was greater in open-water growers (i.e., −70% in *C. gelidus* vs. −14% in *N. frigida*) (Supporting Information Table S5). In all species, the xanthophyll pigment pool size was roughly twice as large under 50 compared to 15 μmol photons m^{-2} s^{-1}, but with greater de-epoxidation state in *F. cylindrus* and *T. gravida* (Fig. 2). Content of the accessory pigments Chl *c* and fucoxanthin were lower under 50 compared to 15 μmol photons m^{-2} s^{-1} in *F. cylindrus* and *C. neogracilis* (Fig. 2), the taxa with the smallest biovolumes (Table 1). Accessory pigments content was mostly unaffected by growth light levels in *N. frigida* and *C. gelidus*, while in *T. gravida*, Chl c_2 content was significantly higher ($P < 0.05$) under 50 compared to 15 μmol photons m^{-2} s^{-1} (Supporting Information Table S5).

Photosynthetic parameters

The dark-adapted quantum yield of photosystem II (F_V/F_M) was generally smaller under 50 than 15 μmol photons m^{-2} s^{-1}, with *F. cylindrus* and *T. gravida* showing lower values than other species (Table 2). The photoacclimation parameter E_k normalized to growth light intensity (E_k/gE) was above 1 in all species under 15 μmol photons m^{-2} s^{-1} (ranging from 2.0 [*N. frigida*] to 5.9 [*C. neogracilis*]), showing none of the species fully acclimated their light response for relative electron transport down to 15 μmol photons m^{-2} s^{-1}. In contrast, E_k/gE was above 1 under 50 μmol photons m^{-2} s^{-1} only in the open-water *C. neogracilis* (2.8) and *C. gelidus* (1.7), indicating light saturation of photosynthetic electron transport under 50 μmol photons m^{-2} s^{-1} in the sympagic (*N. frigida*, *F. cylindrus*) and marginal ice zone (*T. gravida*) species. When E_k was not normalized by growth light, *T. gravida* was the only species that did not show a significant difference ($P > 0.05$) between the two growth light levels (~ 33 μmol photons m^{-2} s^{-1}; Supporting Information Table S6).

Plasticity vs. growth light of NPQ and xanthophyll cycle induction upon light shift

Under 15 μmol photons m^{-2} s^{-1}, the lowest maximal ϕNPQ values were obtained in *N. frigida* and *T. gravida* (~ 0.46), the highest in the *Chaetoceros* species (~ 0.69) with *F. cylindrus* in between (0.56) (Fig. 3, Table 2, ϕNPQ_M). Maximal ϕNPQ value was higher in all species when grown under 50 compared to 15 μmol photons m^{-2} s^{-1}, reflecting larger xanthophyll pigment pools (Fig. 2). The 1.6-fold higher maximal ϕNPQ value in *N. frigida* under 50 compared to 15 μmol photons m^{-2} s^{-1} was the largest difference measured, while *T. gravida* expressed the narrowest difference in maximal ϕNPQ value between growth light levels. Under both growth light levels, the irradiance induction shape of ϕNPQ normalized over the photoacclimation parameter was similar for all species (i.e., $E50\phi NPQ/E_k$ remained between 2 and 2.5), except in *T. gravida* grown under 50 μmol photons m^{-2} s^{-1} (~ 1.6) (Table 2). Under both growth light levels, the *Chaetoceros* species showed sigmoidal ϕNPQ inductions less initially sensitive to lower light levels than the other species (Supporting Information Table S6, higher $E50\phi NPQ$ and $n\phi NPQ$).

Up to a threshold varying between ~ 0.30 (*T. gravida* [under 15 μmol photons m^{-2} s^{-1}]) and ~ 0.79 (*C. gelidus* [under 50 μmol photons m^{-2} s^{-1}]), ϕNPQ was linearly correlated with the newly generated diatoxanthin (ΔDT) (Fig. 3e,f). The initial slopes of ϕNPQ vs. ΔDT were lower in species of smaller size, *F. cylindrus* and *C. neogracilis*, which also had the highest maximal ΔDT (Table 2, ΔDT_M) and de-epoxidation state (Supporting Information Fig. S8, ΔDES_M) under both growth light levels. Slopes of ϕNPQ vs. ΔDT were approximately twofold lower under 50 than 15 μmol photons m^{-2} s^{-1} across all species (Fig. 3). As reported before (Lavaud and Lepetit 2013), a break in the linear relationship of ϕNPQ vs. ΔDT was noticeable at higher light steps as ϕNPQ became saturated before the generation of new diatoxanthin did (i.e., Table 2, $E50\phi NPQ/E50\Delta DT$ below 1). Under growth at 15 μmol photons m^{-2} s^{-1}, this break in ϕNPQ vs. ΔDT was only noticeable in *F. cylindrus* (Fig. 3e), but *N. frigida* and *C. neogracilis* also showed a similar break in ϕNPQ vs. ΔDT under 50 μmol photons m^{-2} s^{-1} (Fig. 3f). A second pattern of nonlinearity was increasing ϕNPQ once the generation of new diatoxanthin became saturated. Under 15 μmol photons m^{-2} s^{-1}, all species except *F. cylindrus* showed this nonlinear ϕNPQ vs. ΔDT pattern (Fig. 3e), but under 50 µmol photons m^{-2} s^{-1}, only *T. gravida* and *C. gelidus* showed this nonlinear pattern (Fig. 3f).

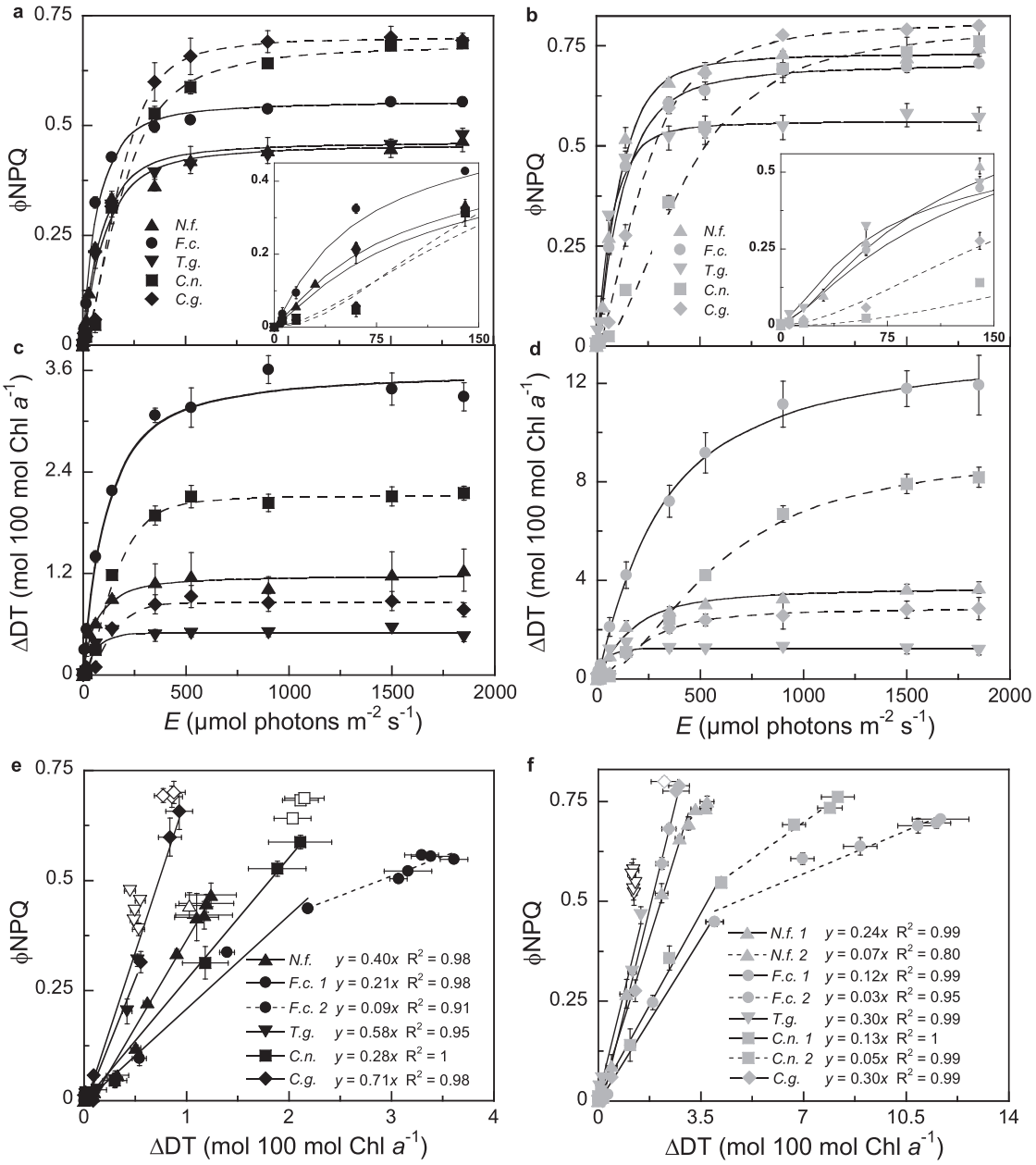

Fig. 3. (**a**, **b**) Nonphotochemical quenching yield (ϕNPQ) and (**c**, **d**) newly generated diatoxanthin (ΔDT) induction measured during nonsequential light curves in all species (species abbreviations are in Table 1) acclimated to growth light (*gE*) of 15 (left panels, black symbols) or 50 μmol photons m^{-2} s^{-1} (right panels, gray symbols). Ice-related and open-water species are distinguished by continuous and dashed lines, respectively. (**e**, **f**) Linear correlations between ϕNPQ and ΔDT. Dashed lines and open symbols represent two patterns of departure from typical ϕNPQ vs. ΔDT linear slope (*see* "Discussion" section), the second equation in some species refers to the dashed line slope. Data are mean values $N = 3$, ± SE. See Table 2 for fitted ϕNPQ or ΔDT nonsequential light curves parameters value, Supporting Information Table S7 for interspecies parameters statistic tests results and Supporting Information Fig. S8 for de-epoxidation state kinetics.

Differences in photophysiological features align with species light niche

Statistical tests comparing photoacclimation and light curve parameter values across species highlight sharp contrasts between species when regrouped by habitat/light niche: sympagic/marginal ice zone (*N. frigida*, *F. cylindrus*, and *T. gravida*, together referred as ice-related species) vs. open-water species (*C. neogracilis* and *C. gelidus*) (Supporting Information Table S7). Open-water species growth rates and photosynthetic parameters (F_V/F_M, E_k/gE) were generally significantly higher ($P < 0.05$) when compared to the ice-related species. Open-water species also had stronger maximal ϕNPQ value, but their induction of ϕNPQ was less initially reactive to lower light level exposure (higher *E50*ϕNPQ and *n*ϕNPQ). Differences in pigment

composition corresponding to light niche were also apparent with lower de-epoxidation state and fucoxanthin content in open-water species compared to ice-related species. However, total xanthophyll pigment pool differences were not explained by light niches. Counterintuitively, the effect of growth light on de-epoxidation state was not significant across species, likely because *N. frigida* had a surprising lower de-epoxidation state under 50 than 15 μmol photons m^{-2} s^{-1}, due to higher diadinoxanthin but similar diatoxanthin content under 50 compared to 15 μmol photons m^{-2} s^{-1} (Fig. 2). Xanthophyll cycle parameters did not vary with species light niches (Supporting Information Table S7) as higher maximal ϕNPQ value was a poor predictor of higher maximal newly generated diatoxanthin across species (Fig. 3). Interaction between the two factors, species and growth light, was significant ($P < 0.01$) for all parameters (except the light for half-saturation of ϕNPQ over newly generated DT [*E50*ϕNPQ/*E50*ΔDT, Supporting Information Table S7]).

Strong sustained NPQ in darkness correlated with diatoxanthin in ice-related species

Patterns of NPQ and xanthophyll cycle in darkness also aligned with species light niche occupancy. Sympagic *N. frigida* and *F. cylindrus* displayed strong sustained NPQ linearly correlated to diatoxanthin content in darkness (Fig. 4 and see Supporting Information Fig. S4 for all species/growth lights). A similar trend was observed in the marginal ice zone *T. gravida*, but only when it was previously acclimated to 50 μmol photons m^{-2} s^{-1} (Fig. 4b). In all cases, F_{Vt}/F_{Mt} increased concomitantly with ϕNPQ relaxation over several hours, mainly through F_{Mt} increasing to its maximal value (Supporting Information Fig. S4). Both the amplitudes and durations of F_{Mt} relaxations were larger when species were previously acclimated to 50 (12–24 h) compared to 15 μmol photons m^{-2} s^{-1} (3–12 h). After reaching maximal values, F_{Mt} slightly dropped, reactivating minor ϕNPQ under prolonged darkness, but diatoxanthin concentrations kept decreasing during the complete 48 h of darkness. *Fragilariopsis cylindrus* expressed the largest sustained NPQ (ϕNPQ up to 0.13). When *T. gravida* cells exhibiting sustained NPQ (acclimated to 50 μmol photons m^{-2} s^{-1}) were transferred to 1 μmol photons m^{-2} s^{-1} rather than darkness, both ϕNPQ and diatoxanthin content rapidly reached lower minimal values (Fig. 4b). Following 48 h of darkness, diatoxanthin remained in all species expressing sustained NPQ, generating de-epoxidation state between 1.5% (*N. frigida*) and 13.5% (*T. gravida*), both grown under 50 μmol photons m^{-2} s^{-1} (Supporting Information Fig. S4).

Dark diatoxanthin accumulation correlated to NPQ in planktonic species

In *C. gelidus* previously acclimated to both growth light levels, ϕNPQ declined while F_{Vt}/F_{Mt} increased (Fig. 5a and Supporting Information Fig. S4i) during the first hour of dark incubation. These trends then abruptly reversed, when ϕNPQ rose to 0.34 (gE_{50}) while F_{Vt}/F_{Mt} collapsed. Increasing ϕNPQ was linearly correlated to diatoxanthin accumulation (Fig. 5c),

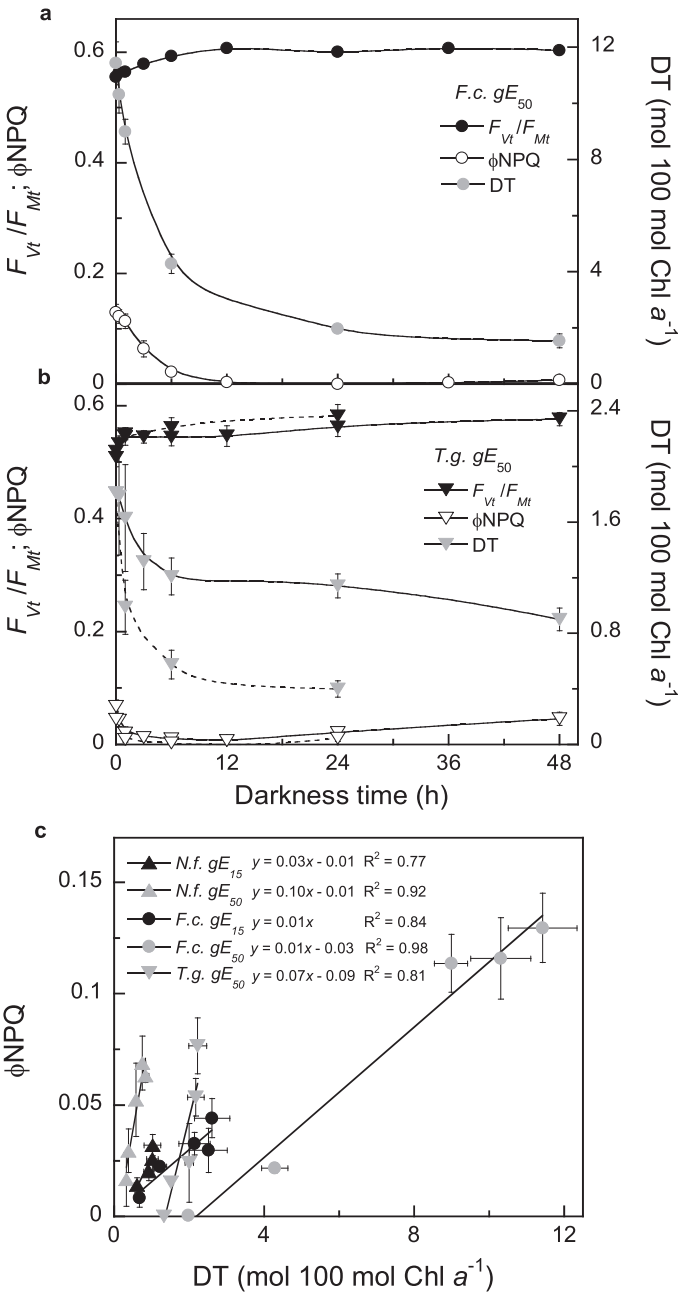

Fig. 4. Sustained nonphotochemical quenching (NPQ_S) relaxation, diatoxanthin (DT) content changes and quantum yield of photosystem II in darkness (F_{Vt}/F_{Mt}) during 48 h dark incubations in (**a**) *Fragilariopsis cylindrus* (*F.c.*) and (**b**) *Thalassiosira gravida* (*T.g.*) previously acclimated to a growth light of 50 μmol photons m^{-2} s^{-1} (gE_{50}); dashed lines in (**b**) represent values measured during parallel 24 h relaxation under 1 μmol photons m^{-2} s^{-1} measured only in *T.g.* (**c**) Linear correlation between NPQ quantum yield (ϕNPQ) and DT content in all species and *gE* combinations for which NPQ_S was observed (species abbreviations are in Table 1). Data are mean values $N = 3$, ± SE. See Supporting Information Fig. S4 for complete fluorescence kinetics and pigment content variations during 48 h dark incubations in all species/*gE*.

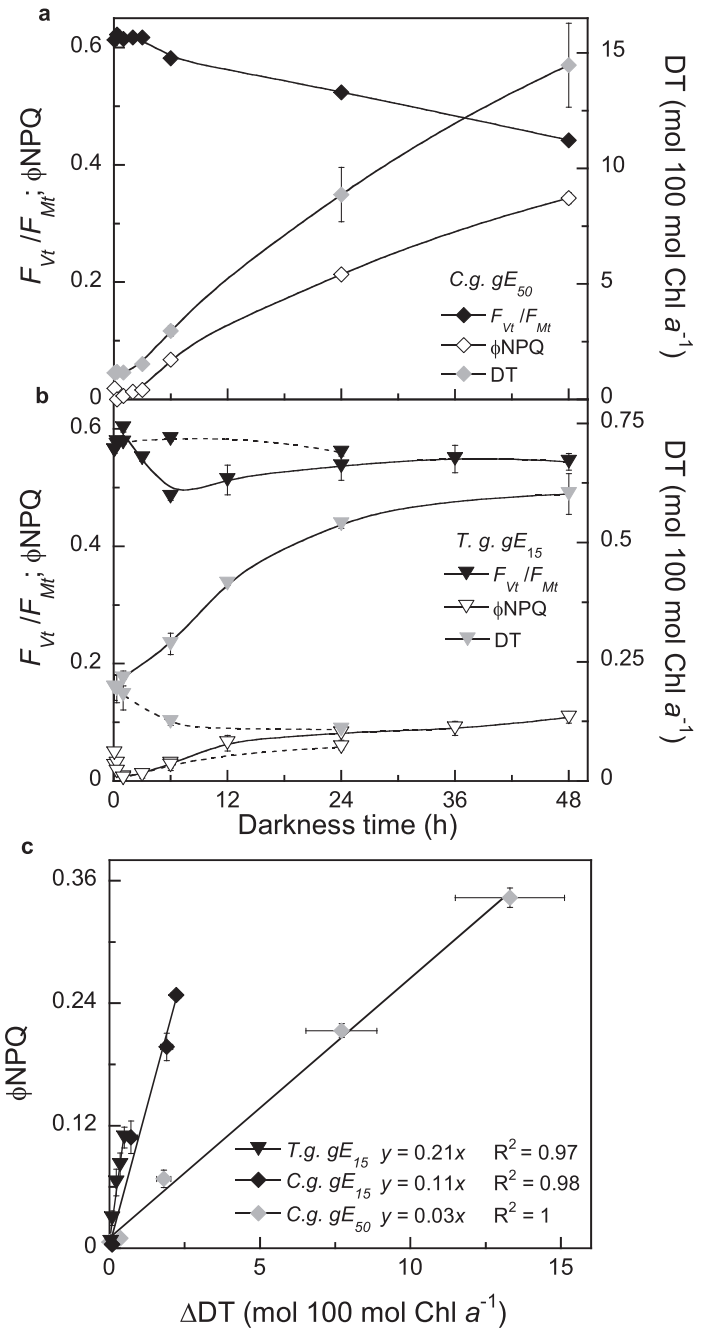

Fig. 5. Dark nonphotochemical yield (ϕNPQ) development, diatoxanthin (DT) content changes and quantum yield of photosystem II in darkness (F_{Vt}/F_{Mt}) during 48 h dark incubations in (**a**) *Chaetoceros gelidus* (*C.g.*) previously acclimated to a growth light of 50 μmol photons m^{-2} s^{-1} (gE_{50}) and (**b**) *Thalassiosira gravida* (*T.g.*) previously acclimated to a growth light of 15 μmol photons m^{-2} s^{-1} (gE_{15}); dashed lines in (**b**) represent values measured during parallel 24 h relaxation under 1 μmol photons m^{-2} s^{-1} measured only in *T.g.* (**c**) Linear correlation between ϕNPQ and newly generated (Δ) DT in all species and *gE* combinations for which darkness ΔDT accumulation was observed (species abbreviations are in Table 1). Data are mean values $N = 3$, ± SE. See Supporting Information Fig. S4 for complete fluorescence kinetics and pigment content variations during 48 h dark incubations in all species/*gE*.

which in turn generated elevated de-epoxidation state (up to 69% [under 50 μmol photons m^{-2} s^{-1}]) (Supporting Information Fig. S4s,t). Diatoxanthin content increased via diadinoxanthin conversion, but a total xanthophyll pigment pool increase (~ 70%) under 50 μmol photons m^{-2} s^{-1} also indicated de novo xanthophyll pigment synthesis (Supporting Information Fig. S4t). *Thalassiosira gravida* previously acclimated to 15 μmol photons m^{-2} s^{-1} showed similar trends (except for the de novo diatoxanthin synthesis) but with lower ϕNPQ (0.11) and de-epoxidation state (16%) (Fig. 5b). In *C. neogracilis*, kinetics were slower. No (under 15 μmol photons m^{-2} s^{-1}) or very low (under 50 μmol photons m^{-2} s^{-1}) initial diatoxanthin amounts were measured, but a modest ϕNPQ nonetheless relaxed during 6–24 h depending upon growth light intensity (Supporting Information Fig. S4g,h). Under 50 μmol photons m^{-2} s^{-1}, diatoxanthin accumulation started after 12 h of darkness and continued steadily thereafter, while a ~ 50% decrease in total xanthophyll pigment revealed a net loss of diadinoxanthin (Supporting Information Fig. S4r).

Discussion

We performed the first systematic investigation of Arctic diatom complementary light and dark NPQ components over a panel of species and deciphered the relationships between NPQ patterns and the xanthophyll cycle. To address gaps in knowledge, we selected five species from contrasting light niches over spring-to-summer habitat transformation (Fig. 1), spanning large ecodiversity in life-traits (Table 1). We revealed strong contrasts in NPQ and xanthophyll cycle patterns which align with the species light niche occupancy. We now discuss how the differential expressions of a suite of photoadaptative features could be of evolutionary value in the species respective light niches (Fig. 6).

Low growth rate and strong photoprotective features in sympagic species

Sympagic species like *N. frigida* and *F. cylindrus* (Figs. 1, 6) initially exploit very weak irradiances early in spring which gradually increase to supersaturating intensities as snow melts (Galindo et al. 2017). In *N. frigida* and *F. cylindrus* low growth rates and ratio of photoacclimation irradiance over 50 μmol photons m^{-2} s^{-1} growth light irradiance (E_k/gE_{50}) below 1 reflect their adaptation to both cold temperatures and dimly lit bottom sea-ice (Lacour et al. 2017). Photoprotective traits like xanthophyll pigment pool size and maximal ϕNPQ showed great plasticity in these sympagic species and were much higher under 50 than under 15 μmol photons m^{-2} s^{-1}. Similar acclimation processes are observed in situ concomitantly with decreasing snow thickness (Galindo et al. 2017). Although maximal ϕNPQ values were smaller in sympagic species than in open-water Arctic species, it still reached high values compared to temperate diatom strains (Barnett et al. 2015) (Stern-Volmer NPQ values are shown in Supporting

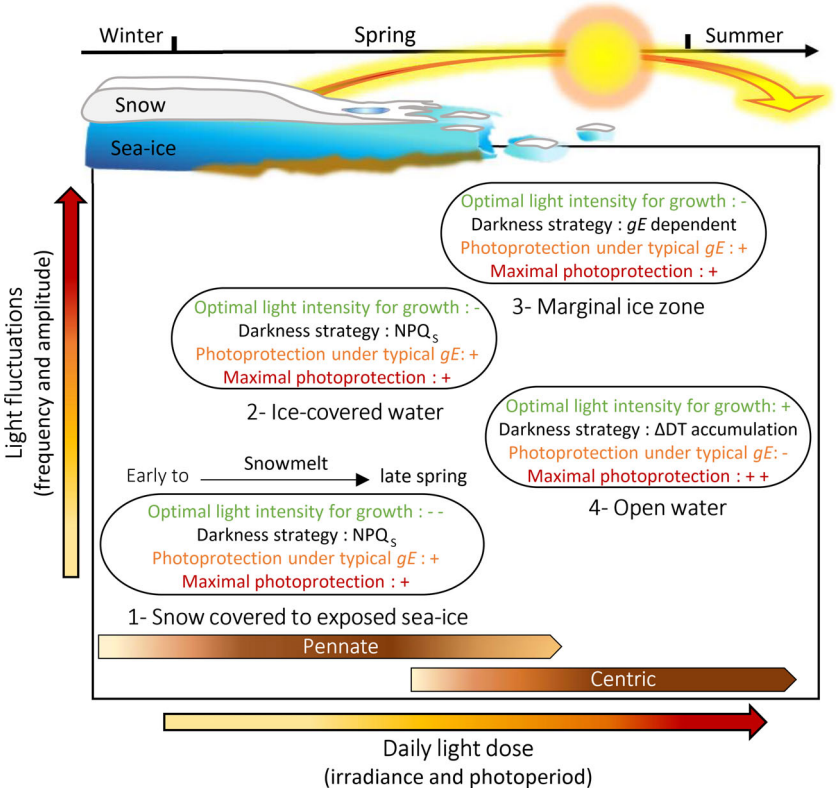

Fig. 6. Cartesian coordinates of four habitats parameterized by daily light dose (*x*-axis) and light fluctuations (*y*-axis), with hypothesized adaptations to the light climate for four photophysiological features (optimal light level for growth [μ, *Ek*/*gE*], darkness strategy, photoprotection under typical growth light level [*E50*ϕNPQ/*gE*, *n*ϕNPQ, *E50*ΔDT/*gE*], and maximal fast photoprotection [ϕNPQ_M, ΔDT_M]) in diatom species thriving in these niches. Transition between habitats, light climate progression and pennate-to-centric dominated diatom communities shift are part of the Arctic Ocean seasonal dynamics described in the introduction, Fig. 1, and Supporting Information Fig. S1. *gE*, growth light; NPQ_S, sustained nonphotochemical quenching; ΔDT, newly generated diatoxanthin. The habitats of the species studied are found in Table 1, the parameters in parenthesis representing photophysiological features are defined in Supporting Information Table S3, their observed values in the species studied are found in Table 2 and Supporting Information Table S6, and interspecies statistic tests results in Supporting Information Table S7. Adapted from Dimier et al. (2009).

Information Fig. S9 for comparison purposes with earlier studies). Logarithmic, as opposed to sigmoidal, ϕNPQ induction ($n\phi NPQ < 2$) triggered by light even lower than their growth light level, shows that sea-ice species regulated absorbed light dissipation even before photosynthesis saturates. However, in all species and for all growth light levels combinations, photoprotection was tuned to photochemical potential as light shifted to saturating intensities (i.e., ~ 2.2 $E50\phi NPQ/E_k$, Supporting Information Table S6) (Lepetit et al. 2013).

The slope of ϕNPQ vs. the newly generated diatoxanthin (ΔDT) is an important photoadaptative feature which is usually steeper in species adapted to more dynamic light climates (Lavaud and Lepetit 2013). In our study, sympagic *F. cylindrus* and *N. frigida* expressed among the smallest ϕNPQ vs. ΔDT slopes, which could illustrate adaptation to slower light fluctuations in bottom sea-ice compared to the faster light fluctuations in the water column. While ϕNPQ vs. ΔDT reflects the diatoxanthin proportion directly involved in NPQ-*qE*, diatoxanthin can play alternative photoprotective purposes under increasing light including: (1) Temperature-sensitive thylakoid membrane stabilizer (Bojko et al. 2019); and (2) Scavenging of oxidative radicals (Smerilli et al. 2019). Involvement of diatoxanthin in such functions would promote lower ϕNPQ vs. ΔDT and a departure from linearity under saturating light exposure, as indeed observed in *N. frigida* (under 50 μmol photons m^{-2} s^{-1}) and *F. cylindrus*. Antioxidant DT could facilitate survival over sea-ice thawing/freezing cycles which generate hyperoxia and salinity oscillations which can inhibit photosynthetic capacities (McMinn et al. 2005).

Sustained NPQ in sea-ice related species: An adaptation to seasonal light overdose in a freezing environment?

Alongside strong NPQ-*qE* plasticity, sustained NPQ could complement adaptation to late spring excessive light in sea-ice habitats. Locked-in photoprotection in darkness is typically observed in organisms coping with chronic disequilibrium between light harvesting and carbon fixing capacities, like overwintering evergreen trees in which cold slows down the Calvin-Benson cycle enzymes (Verhoeven et al. 2018). In these trees, the loss of carbohydrate sinks triggers a sustained NPQ-like

response, supporting the hypothesis of a light harvesting dimmer function, regulated by feedback from carbon utilization rate (Adams et al. 2014). Notably, in our study, those species expressing sustained NPQ (*N. frigida*, *F. cylindrus*, and *T. gravida*) did not grow faster under 50 compared to 15 μmol photons m^{-2} s^{-1}, and showed acclimative responses to decrease light harvesting under 50 μmol photons m^{-2} s^{-1} (lower Chl *a*, higher *E50*ϕNPQ/*gE*); hence their growth is likely limited by downstream carbon metabolism rather than by light above 15 μmol photons m^{-2} s^{-1}. Importantly, our finding reinforces that sustained NPQ is not an oddity found in select polar species or relevant only under stress conditions (Lacour et al. 2018), but rather a widespread feature in ice-related taxa.

Sustained NPQ in darkness in diatoms is usually attributed to diatoxanthin molecules remaining bound to disconnected light-harvesting complexes, preventing full NPQ relaxation (Goss and Lepetit 2015). The enzymatic diatoxanthin back conversion to diadinoxanthin is possibly inhibited by a shortage of NADPH cofactor, via transient plastid to mitochondria NADPH/ATP translocations upon light to darkness shift (Barnett et al. 2015). This is supported by the faster diatoxanthin epoxidation and sustained NPQ relaxation under 1 μmol photons m^{-2} s^{-1} (*T. gravida* acclimated to 50 μmol photons m^{-2} s^{-1}, Fig. 4b) which allows some generation of NADPH in the chloroplast. Additionally, sustained NPQ exacerbated under 50 compared to 15 μmol photons m^{-2} s^{-1} could result from upregulation of mitochondrial excess-energy sinks influencing NADPH availability in the chloroplast, such as photorespiration or the ornithine-glutamine shunt (Broddrick et al. 2019). In contrast to Lacour et al. (2018), sustained NPQ was not completely correlated to diatoxanthin, supporting our proposal of a diatoxanthin fraction not participating in NPQ (see biphasic ϕNPQ vs. ΔDT slopes; Fig. 3e,f) and governed by longer time scale reactions in ice-related species. Notably, the recent report that in plant long-lasting quenching, zeaxanthin (de-epoxidized xanthophyll in plants analogous to diatoxanthin) serves a "molecular memory" role controlling allosteric modulation of long-term quenching (Kress and Jahns 2017). The "molecular memory hypothesis" has also been proposed to explain strong NPQ maintenance in sea-ice microalgae 2 weeks following a snowfall-induced darkness event (Galindo et al. 2017). Finally, we cannot exclude that differential LHCx proteins expression among species and growth light combinations could partly explain contrasting sustained NPQ kinetics. The LHCx family is extensively diversified in polar diatoms (Mock et al. 2017) including isoform(s) that are specifically dark upregulated (Goss and Lepetit 2015).

Faster growth and contrasting depth adaptation in open-water species

Open-water *C. neogracilis* and *C. gelidus* (Figs. 1, 6) exploit a dynamic light environment defined by niche depth and two overlapping seasonal phenomena: (1) light fluctuation amplitude gradually diminishes from spring to summer as the stratification of the surface layer dampens vertical mixing; and (2) daily irradiance evolves with increasing photoperiod and solar angle-of-incidence. Open-water species success relies on quickly maximizing productivity to consume declining nutrient pools and outgrow zooplankton grazing (Mayot et al. 2018). Open-water *Chaetoceros* species showed stronger photoprotective capacities under higher growth light, like their ice-related diatom counterparts, but additionally faster growth rates and ratio of photoacclimation irradiance over 50 μmol photons m^{-2} s^{-1} growth light irradiance (E_k/*gE*) above 1 (Table 2). Their sigmoidal NPQ induction (nϕNPQ > 2) was triggered by light slightly above growth irradiance, allowing maintenance of efficient light harvesting under mild light fluctuations, which is likely advantageous as water warms and gradually boosts photosynthetic enzyme kinetics.

Chaetoceros species showed similarly high maximal ϕNPQ but contrasting xanthophyll cycle kinetics upon light shifts (Fig. 3), possibly explained by their differential depth adaptation (Ocampo-alvarez and García-mendoza 2013) (Table 1). Via vertical mixing, the deeper niche adapted *C. gelidus* is prone to larger light fluctuations than *C. neogracilis* dwelling in surface waters. As explained above, such conditions could well promote stronger ϕNPQ vs. ΔDT in *C. gelidus* than in *C. neogracilis*. Interestingly, in *C. neogracilis* previously acclimated to 50 μmol photons m^{-2} s^{-1}, a biphasic ϕNPQ vs. ΔDT relationship resembled the one in *F. cylindrus*. Additionally, both strains exhibited a similar decrease in the ratio of the light for half-saturation of NPQ induction over growth light level (*E50*ϕNPQ/*gE*) between 15 and 50 μmol photons m^{-2} s^{-1} light acclimation (Table 2). Although our overall observations link *F. cylindrus* more to an ice-related photoadaptation strategy, *F. cylindrus* can also be found abundantly in surficial meltwaters (Lafond et al. 2019) and its high light acclimation on longer timescales (Kropuenske et al. 2009) or coupled with temperature and salinity changes (Petrou et al. 2011) have also revealed strong adaptation to stratified surface layers in this bipolar species. Similarities between *C. neogracilis* and *F. cylindrus* could also be explained by trade-off with their small biovolume (Table 1) leaving them more vulnerable to photosystem II photoinactivation due to lower internal self-shading (Key et al. 2010); note the opposing sharpest ϕNPQ vs. ΔDT in the very large *T. gravida*. Thus, in addition to their light niche adaptation, smaller species may invest more in xanthophyll pigments supporting NPQ-*qE* photoprotection to limit photoinactivation (Smerilli et al. 2019). Interestingly, an Antarctic field survey found a strong correlation between a decrease in cellular volume and a larger xanthophyll pigment pool content per Chl *a* (Ferreira et al. 2017).

Strong xanthophyll content modulations drive open-water species dark acclimation

A deeper niche makes *C. gelidus* more prone to mixing out of the photic zone and may also explain its more dynamic dark response with strong NPQ and xanthophyll cycle induction. A similar, but much slower pattern, visible here in

50 μmol photons m^{-2} s^{-1} cells after 24 h darkness (Supporting Information Fig. S4r), was reported in *C. neogracilis* (Lacour et al. 2019), as well as in temperate phytoplankton (Brunet et al. 2007). In these studies, a chlororespiration-generated proton gradient was hypothesized to activate dark NPQ and diadinoxanthin de-epoxidation. Strong dark de novo synthesis of xanthophyll pigment (Supporting Information Fig. S4t), with a significant increase ($P < 0.05$) in β-carotene (the precursor for xanthophylls) (Supporting Information Fig. S10a), in *C. gelidus* 50 μmol photons m^{-2} s^{-1} is in line with this hypothesis as carotenoid biosynthesis requires plastoquinone-pool oxidation possibly mediated via chlororespiration in darkness (Ruiz-Sola and Rodríguez-Concepción 2012). Also noteworthy is the gene transcription for plastid terminal oxidase (the central enzyme in chlororespiration) under variable light and iron conditions in several polar diatoms (Moreno et al. 2018). However, diatoms' dark metabolism is complex (Bailleul et al. 2015) and several reductant routing pathways toward mitochondria could oxidize the plastoquinone-pool (Broddrick et al. 2019), making it difficult to pinpoint a sole process (chlororespiration) as explaining the dark diatoxanthin accumulation and NPQ increased observed here in *C. gelidus*. Additionally, we measured a significant decrease ($P < 0.05$) of the total xanthophyll pigment pool concomitant to increasing fucoxanthin content in *C. neogracilis* in darkness previously acclimated to 50 μmol photons m^{-2} s^{-1} (Supporting Information Fig. S10b), reinforcing a possible important role of nonphotosynthetic reactions in regulating carotenoid synthesis in diatoms. This novel observation is of much interest to fucoxanthin's debated synthesis pathway (Dautermann et al. 2020). Although the nature of these dark processes remains to be investigated, they hint at a complex and active metabolism in darkness (Kennedy et al. 2019), likely facilitating photochemistry engagement upon reillumination (Lacour et al. 2019; Morin et al. 2020).

Expanded light and dark response plasticity in marginal ice zone species

Marginal ice zone bloomers like *T. gravida* must exploit flickering light generated by the fragmenting sea-ice cover (Figs. 1, 6). While the lowest performer in terms of maximal ϕNPQ, *T. gravida* showed the steepest ϕNPQ vs. ΔDT slopes, which could reflect adaptation to frequent and erratic light fluctuations of large amplitude (Lavaud and Lepetit 2013). Additionally, *T. gravida* was the sole taxa capable of lowering the ratio of the light for half-saturation of NPQ induction over the photoacclimation parameter ($E50\phi NPQ/E_k$) under 50 compared to 15 μmol photons m^{-2} s^{-1} (Table 2). This illustrates its strong capacity to optimize ϕNPQ induction vs. photochemical potential as a function of light history, an important attribute to exploit the unsteady light climate of the marginal ice zone. Although, *T. gravida* photoadaptation is not primarily constrained by extremophile growth in brine channels, it experiences a yearly light cycle similar to sympagic species. Ice-related species take advantage of snow/sea-ice shading early in the season before being exposed to supersaturating irradiances when sea-ice is denuded of snow or they are trapped in stratified meltwaters (or both in the case of *F. cylindrus* case). Adaptation to such a habitat transition could explain the strikingly similar acclimation to stronger irradiance (*see* Supporting Information Table S7 and development of sustained NPQ; Fig. 4) between the marginal ice zone associated *T. gravida* and the sympagic species (*N. frigida*, *F. cylindrus*).

The dark response in *T. gravida*, alone, was growth irradiance-dependent: dark diatoxanthin accumulation similar to open-water species under 15 μmol photons m^{-2} s^{-1} (Fig. 5b) vs. sympagic-like sustained NPQ under 50 μmol photons m^{-2} s^{-1} (Fig. 4b). The partitioning of NADPH could be the pivotal factor between these two strategies as (Goss and Lepetit 2015): (1) NADPH depletion inhibits diatoxanthin epoxidation to diadinoxanthin which supports sustained NPQ; and (2) NADPH accumulation in the stroma could feed a proton pumping dehydrogenase generating a proton gradient required for NPQ and xanthophyll cycle induction. Possibly, a tipping point between these two situations is reached between the two growth light levels used here for *T. gravida*, which is plausible considering its niche on the fringe between sea-ice and open-water. Expanding this reasoning to the other taxa studied, they might all potentially express sustained NPQ or diatoxanthin accumulation in darkness depending on the preceding growth light relative to a species-specific photoadaptation range. For example, sustained NPQ may also be observable in open-water diatoms but triggered by a higher light dose than in shade-adapted sympagic species. Nevertheless, how metabolic fine-tuning could induce such exacerbated NPQ and xanthophyll cycle reactions in Arctic diatoms compared to temperate counterparts remains to be investigated. Alternatively, because xanthophyll cycle and NPQ dark induction stalled when *T. gravida* acclimated to 15 μmol photons m^{-2} s^{-1} was transferred under 1 μmol photons m^{-2} s^{-1} (Fig. 5b), it is possible darkness biases xanthophyll cycle toward net diatoxanthin conversion. Likewise, *Phaeomonas* sp. shows maximal xanthophyll epoxidation under moderate light, and therefore, strong NPQ and diatoxanthin generation triggered by both darkness and high light (Berne et al. 2018).

Independent of the sympagic/sustained NPQ and open-water/dark diatoxanthin accumulation strategy dichotomy highlighted in this study, fast reactivation of photosynthesis after prolonged darkness (month[s] scale) is common in polar diatoms (Kvernvik et al. 2018; Morin et al. 2020). Gene-level assessment of polar night acclimation in open-water species, as has been conducted on *F. cylindrus* (Kennedy et al. 2019), could reveal crucial details on the evolution of divergent dark metabolic patterns.

Concluding remarks

NPQ and the underlying xanthophyll cycle are keystone components of species-specific photoadaptative strategies in most microalgae groups (Lacour et al. 2020), allowing them to

cope with changing light conditions and deeply influencing the global carbon cycle (Álvarez et al. 2019). Our study describes similar photoadaptation patterns across Arctic diatoms from different light niches, but surprisingly, also reveals contrasts in the dark regulation of these photoprotective mechanisms across niches (Supporting Information Fig. S4). We propose unusual NPQ and xanthophyll cycle dark patterns could be Arctic diatoms' evolved response to an extreme climate, where light availability is severely constrained by interactions of sea-ice cycles, photoperiod, and solar angle.

We use our analysis of NPQ and xanthophyll cycle diversity and photoacclimation patterns as initial steps toward a refined resolution of Arctic diatom photoadaptation strategies with respect to their light niches (Fig. 6) in a framework to be expanded to include complementary photophysiological processes of longer term photoacclimation, carbon fixation, and the photosystem II repair cycle (Croteau et al. unpubl.). We believe these results will help field campaign data interpretation, for example, ice-core vs. water column samples, as well as analytic and predictive modeling efforts amid the ongoing intensification of the Arctic Ocean's light climate. We suggest a similar lab-controlled niche resolved approach would be valuable to apprehend Arctic diatom adaptations to other shifting environmental gradients in the context of climate change (see for instance, Kvernvik et al. 2020 for ocean acidification, and Petrou et al. 2011 for temperature and salinity in Antarctic species). Future Arctic trophic webs and biogeochemical cycle dynamics will greatly depend on how indigenous and/or poleward advected Atlantic phototrophic species (Oziel et al. 2020) adjust to increasing energy (light and heat) and matter (carbon and nutrients) influx. Heterogeneous Arctic diatom NPQ and xanthophyll cycle adaptations to contrasting light niches will likely yield divergent responses to abruptly transforming physicochemical matrices.

References

Adams, W. W., O. Muller, C. M. Cohu, and B. Demmig-Adams. 2014. Photosystem II efficiency and non-photochemical fluorescence quenching in the context of source-sink balance, p. 503–529. *In* B. Demmig-Adams, W. W. Adams, and A. K. Mattoo [eds.], Photoprotection, photoinhibition, gene regulation, and environment. Advances in photosynthesis and respiration. Springer.

Álvarez, E., S. Thoms, A. Bracher, Y. Liu, and C. Völker. 2019. Modeling photoprotection at global scale: The relative role of non-photosynthetic pigments, physiological state and species composition. Global Biogeochem. Cycles **33**: 904–926. doi:10.1029/2018GB006101

Arrigo, K. R., and others. 2012. Massive phytoplankton plooms under Arctic Sea ice. Science **336**: 1408. doi:10.1126/science.1215065

Bailleul, B., and others. 2015. Energetic coupling between plastids and mitochondria drives CO_2 assimilation in diatoms. Nature **524**: 366–369. doi:10.1038/nature14599

Balzano, S., I. Percopo, R. Siano, P. Gourvil, M. Chanoine, D. Marie, D. Vaulot, and D. Sarno. 2017. Morphological and genetic diversity of Beaufort Sea diatoms with high contributions from the *Chaetoceros neogracilis* species complex. J. Phycol. **53**: 161–187. doi:10.1111/jpy.12489

Barnett, A. V., and others. 2015. Growth form defines physiological photoprotective capacity in intertidal benthic diatoms. ISME J. **9**: 32–45. doi:10.1038/ismej.2014.105

Berne, N., T. Fabryova, F. Bistaz, P. Cardol, and B. Bailleul. 2018. The peculiar NPQ regulation in the stramenopile *Phaeomonas* sp. challenges the xanthophyll cycle dogma. Biochim. Biophys. Acta Bioenerg. **1859**: 491–500. doi:10.1016/j.bbabio.2018.03.013

Bojko, M., M. Olchawa-Pajor, R. Goss, S. Schaller-Laudel, K. Strzałka, and D. Latowski. 2019. Diadinoxanthin de-epoxidation as important factor in the short-term stabilization of diatom photosynthetic membranes exposed to different temperatures. Plant Cell Environ. **42**: 1270–1286. doi:10.1111/pce.13469

Broddrick, J. T., and others. 2019. Cross-compartment metabolic coupling enables flexible photoprotective mechanisms in the diatom *Phaeodactylum tricornutum*. New Phytol. **222**: 1364–1379. doi:10.1111/nph.15685

Brunet, C., R. Casotti, V. Vantrepotte, and F. Conversano. 2007. Vertical variability and diel dynamics of picophytoplankton in the Strait of Sicily, Mediterranean Sea, in summer. Mar. Ecol. Prog. Ser. **346**: 15–26. doi:10.3354/meps07017

Buck, J. M., and others. 2019. Dissipation of absorbed light in the diatom *Phaeodactylum tricornutum*. Nat. Commun. **10**: 1–12. doi:10.1038/s41467-019-12043-6

Campbell, D. A., and J. Serôdio. 2020. Photoinhibition of photosystem II in phytoplankton: Processes and patterns, p. 329–365. *In* A. Larkum, A. Grossmann, and J. Raven [eds.], Photosynthesis in algae: Biochemical and physiological mechanisms. Advances in photosynthesis and respiration (including bioenergy and related processes). Springer.

Dautermann, O., and others. 2020. An algal enzyme required for biosynthesis of the most abundant marine carotenoids. Sci. Adv. **6**: eaaw9183. doi:10.1126/sciadv.aaw9183

Dimier, C., S. Giovanni, T. Ferdinando, and C. Brunet. 2009. Comparative ecophysiology of the xanthophyll cycle in six marine phytoplanktonic species. Protist **160**: 397–411. doi:10.1016/j.protis.2009.03.001

Ferreira, A., A. M. Ciotti, C. R. B. Mendes, J. Uitz, and A. Bricaud. 2017. Phytoplankton light absorption and the package effect in relation to photosynthetic and photoprotective pigments in the northern tip of Antarctic Peninsula. J. Geophys. Res. Oceans **122**: 7344–7463. doi:10.1002/2017JC012964

Galindo, V., M. Gosselin, J. Lavaud, C. J. Mundy, B. Else, J. Ehn, M. Babin, and S. Rysgaard. 2017. Pigment

composition and photoprotection of Arctic Sea ice algae during spring. Mar. Ecol. Prog. Ser. **585**: 49–69. doi:10.3354/meps12398

Goss, R., and B. Lepetit. 2015. Biodiversity of NPQ. J. Plant Physiol. **172**: 13–32. doi:10.1016/j.jplph.2014.03.004

Hancke, K., L. C. Lund-Hansen, M. L. Lamare, S. Højlund Pedersen, M. D. King, P. Andersen, and B. K. Sorrell. 2018. Extreme low light requirement for algae growth underneath sea ice: A case study from Station Nord, NE Greenland. J. Geophys. Res. Oceans **123**: 985–1000. doi:10.1002/2017JC013263

Katlein, C., S. Arndt, H. J. Belter, G. Castellani, and M. Nicolaus. 2019. Seasonal evolution of light transmission distributions through Arctic Sea ice. J. Geophys. Res. Oceans **124**: 5418–5435. doi:10.1029/2018JC014833

Kennedy, F., A. Martin, J. P. Bowman, R. Wilson, and A. McMinn. 2019. Dark metabolism: A molecular insight into how the Antarctic Sea-ice diatom *Fragilariopsis cylindrus* survives long-term darkness. New Phytol. **223**: 675–691. doi:10.1111/nph.15843

Key, T., A. McCarthy, D. A. Campbell, C. Six, S. Roy, and Z. V. Finkel. 2010. Cell size trade-offs govern light exploitation strategies in marine phytoplankton. Environ. Microbiol. **12**: 95–104. doi:10.1111/j.1462-2920.2009.02046.x

Kress, E., and P. Jahns. 2017. The dynamics of energy dissipation and xanthophyll conversion in *Arabidopsis* indicate an indirect photoprotective role of zeaxanthin in slowly inducible and relaxing components of non-photochemical quenching of excitation energy. Front. Plant Sci. **8**: 1–17. doi:10.3389/fpls.2017.02094

Kropuenske, L. R., M. M. Mills, G. L. van Dijken, S. Bailey, D. H. Robinson, N. Welschmeyer, and K. R. Arrigo. 2009. Photophysiology in two major Southern Ocean phytoplankton taxa: Photoprotection in *Phaeocystis antarctica* and *Fragilariopsis cylindrus*. Limnol. Oceanogr. **54**: 1176–1196. doi:10.4319/lo.2009.54.4.1176

Kvernvik, A. C., C. J. M. Hoppe, E. Lawrenz, O. Prášil, M. Greenacre, J. M. Wiktor, and E. Leu. 2018. Fast reactivation of photosynthesis in arctic phytoplankton during the polar night. J. Phycol. **54**: 461–470. doi:10.1111/jpy.12750

Kvernvik, A. C., S. D. Rokitta, E. Leu, L. Harms, T. M. Gabrielsen, B. Rost, and C. J. M. Hoppe. 2020. Higher sensitivity towards light stress and ocean acidification in an Arctic Sea-ice associated diatom compared to a pelagic diatom. New Phytol. **226**: 1708–1724. doi:10.1111/nph.16501

Lacour, T., J. Larivière, and M. Babin. 2017. Growth, Chl *a* content, photosynthesis, and elemental composition in polar and temperate microalgae. Limnol. Oceanogr. **62**: 43–58. doi:10.1002/lno.10369

Lacour, T., J. Larivière, J. Ferland, F. Bruyant, J. Lavaud, and M. Babin. 2018. The role of sustained photoprotective non-photochemical quenching in low temperature and high light acclimation in the bloom-forming Arctic diatom *Thalassiosira gravida*. Front. Mar. Sci. **5**: 1–16. doi:10.3389/fmars.2018.00354

Lacour, T., P. I. Morin, T. Sciandra, N. Donaher, D. A. Campbell, J. Ferland, and M. Babin. 2019. Decoupling light harvesting, electron transport and carbon fixation during prolonged darkness supports rapid recovery upon re-illumination in the Arctic diatom *Chaetoceros neogracilis*. Polar Biol. **42**: 1787–1799. doi:10.1007/s00300-019-02507-2

Lacour, T., M. Babin, and J. Lavaud. 2020. Diversity of xanthophyll cycle pigments content and related non-photochemical quenching (NPQ) among microalgae: Implications for growth strategy and ecology. J. Phycol. **56**: 245–263. doi:10.1111/jpy.12944

Lafond, A., and others. 2019. Late spring bloom development of pelagic diatoms in Baffin Bay. Elem. Sci. Anth. **7**: 44. doi:10.1525/elementa.382

Lavaud, J., and B. Lepetit. 2013. An explanation for the inter-species variability of the photoprotective non-photochemical chlorophyll fluorescence quenching in diatoms. Biochim. Biophys. Acta Bioenerg. **1827**: 294–302. doi:10.1016/j.bbabio.2012.11.012

Lepetit, B., S. Sturm, A. Rogato, A. Gruber, M. Sachse, A. Falciatore, P. G. Kroth, and J. Lavaud. 2013. High light acclimation in the secondary plastids containing diatom *Phaeodactylum tricornutum* is triggered by the redox state of the plastoquinone pool. Plant Physiol. **161**: 853–865. doi:10.1104/pp.112.207811

Leu, E., J. Wiktor, J. E. Søreide, J. Berge, and S. Falk-Petersen. 2010. Increased irradiance reduces food quality of sea ice algae. Mar. Ecol. Prog. Ser. **411**: 49–60. doi:10.3354/meps08647

Lewis, K. M., G. L. van Dijken, and K. R. Arrigo. 2020. Changes in phytoplankton concentration now drive increased Arctic Ocean primary production. Science **369**: 198–202. doi:10.1126/science.aay8380

Massicotte, P., and others. 2020. Green Edge ice camp campaigns: Understanding the processes controlling the under-ice Arctic phytoplankton spring bloom. Earth Syst. Sci. Data **12**: 151–176. doi:10.5194/essd-2019-160

Mayot, N., P. Matra, I. H. Ellingsen, M. Steele, K. Johnson, S. C. Riser, and D. Swift. 2018. Assessing phytoplankton activities in the seasonal ice zone of the Greenland Sea over an annual cycle. J. Geophys. Res. Oceans **123**: 8004–8025. doi:10.1029/2018JC014271

McMinn, A., A. Pankowski, and T. Delfatti. 2005. Effect of hyperoxia on the growth and photosynthesis of polar sea ice microalgae. J. Phycol. **41**: 732–741. doi:10.1111/j.1529-8817.2005.00095.x

Mock, T., and others. 2017. Evolutionary genomics of the cold-adapted diatom *Fragilariopsis cylindrus*. Nature **541**: 536–540. doi:10.1038/nature20803

Moreno, C. M., Y. Lin, S. Davies, E. Monbureau, N. Cassar, and A. Marchetti. 2018. Examination of gene repertoires

and physiological responses to iron and light limitation in Southern Ocean diatoms. Polar Biol. **41**: 679–696. doi:10.1007/s00300-017-2228-7

Morin, P. I., and others. 2020. Response of the sea-ice diatom *Fragilariopsis cylindrus* to simulated polar nigh darkness and return to light. Limnol. Oceanogr. **65**: 1040–1059. doi:10.1002/lno.11368

Ocampo-alvarez, H., and E. García-mendoza. 2013. Antagonist effect between violaxanthin and de-epoxidated pigments in nonphotochemical quenching induction in the qE deficient brown alga *Macrocystis pyrifera*. Biochim. Biophys. Acta Bioenerg. **1827**: 427–437. doi:10.1016/j.bbabio.2012.12.006

Oziel, L., and others. 2020. Faster Atlantic currents drive poleward expansion of temperate phytoplankton in the Arctic Ocean. Nat. Commun. **11**: 1–8. doi:10.1038/s41467-020-15485-5

Petrou, K., M. A. Doblin, and P. J. Ralph. 2011. Heterogeneity in the photoprotective capacity of three Antarctic diatoms during short-term changes in salinity and temperature. Mar. Biol. **158**: 1029–1041. doi:10.1007/s00227-011-1628-4

Polimene, L., C. Brunet, M. Butenschon, V. Martinez-Vicente, C. Widdicombe, R. Torres, and J. I. Allen. 2014. Modelling a light-driven phytoplankton succession. J. Plankton Res. **36**: 214–229. doi:10.1093/plankt/fbt086

Post, E., and others. 2013. Ecological consequences of sea-ice decline. Science **341**: 519–524. doi:10.1126/science.1235225

Poulin, M., N. Daugbjerg, R. Gradinger, L. Ilyash, T. Ratkova, and C. von Quillfeldt. 2011. The pan-Arctic biodiversity of marine pelagic and sea-ice unicellular eukaryotes: A first-attempt assessment. Mar. Biodivers. **41**: 13–28. doi:10.1007/s12526-010-0058-8

Ras, J., H. Claustre, and J. Uitz. 2008. Spatial variability of phytoplankton pigment distributions in the subtropical South Pacific Ocean: Comparison between in situ and predicted data. Biogeosciences **5**: 353–369. doi:10.5194/bg-5-353-2008

Ruiz-Sola, M. Á., and M. Rodríguez-Concepción. 2012. Carotenoid biosynthesis in *Arabidopsis*: A colorful pathway. Arabidopsis Book **10**: e0158. doi:10.1199/tab.0158

Serôdio, J., and J. Lavaud. 2011. A model for describing the light response of the nonphotochemical quenching of chlorophyll fluorescence. Photosynth. Res. **108**: 61–76. doi:10.1007/s11120-011-9654-0

Smerilli, A., S. Balzano, M. Maselli, M. Blasio, I. Orefice, C. Galasso, C. Sansone, and C. Brunet. 2019. Antioxidant and photoprotection networking in the coastal diatom *Skeletonema marinoi*. Antioxidants **8**: 154. doi:10.3390/antiox8060154

Verhoeven, A., J. I. García-plazaola, and B. Fernández-marín. 2018. Shared mechanisms of photoprotection in photosynthetic organisms tolerant to desiccation or to low temperature. Environ. Exp. Bot. **154**: 66–79. doi:10.1016/j.envexpbot.2017.09.012

Acknowledgments

We thank the contribution of CNRS in the framework of the UMI Takuvik, the Canada Excellence Research Chair on *Remote sensing of Canada's new Arctic frontier* (M. Babin), NSERC Canada Discovery grant (RGPIN-2017-04505) (J. Lavaud), the Sentinel North program of Université Laval (Canada First Research Excellence Fund) and the research network Québec-Océan for their financial support; J. Larivière and M. Béguin for their technical support; M. Simard and V. Richard for their support with HPLC; P. Massicotte and N. Schiffrine for their help with statistical analyses and diatom culturing, respectively; M.-H. Forget for her management support, and Profs. A. Juhl and M. Gosselin for kindly providing us with the *N. frigida* strain and the XE-PAM, respectively.

Conflict of Interest

None declared.

Submitted 08 January 2020
Revised 12 June 2020
Accepted 28 July 2020

Associate editor: Ronnie Glud